Magnetic anisotropy and reversal in epitaxial Fe/MgO(001) films

Qing-feng Zhan,[1] Stijn Vandezande,[1] Kristiaan Temst,[2] and Chris Van Haesendonck[1]
[1]*Laboratorium voor Vaste-Stoffysica en Magnetisme and Institute for Nanoscale Physics and Chemistry (INPAC), Katholieke Universiteit Leuven, Celestijnenlaan 200 D, BE-3001 Leuven, Belgium*
[2]*Instituut voor Kern- en Stralingsfysica and Institute for Nanoscale Physics and Chemistry (INPAC), Katholieke Universiteit Leuven, Celestijnenlaan 200 D, BE-3001 Leuven, Belgium*
(Received 30 December 2008; revised manuscript received 16 July 2009; published 24 September 2009)

We investigate the magnetization reversal in Fe/MgO(001) films with fourfold in-plane magnetic anisotropy and an additional uniaxial anisotropy whose orientation and strength are altered using different growth geometries and postgrowth treatments. The previously adopted mechanism of 180° domain-wall nucleation clearly fails to explain the observed 180° magnetization reversal in Fe/MgO(001) films. We introduce a reversal mechanism with two successive domain-wall nucleations to consistently predict the switching fields of Fe/MgO(001) films for all field orientations with one set of values for domain-wall nucleation energies and uniaxial anisotropy.

DOI: 10.1103/PhysRevB.80.094416 PACS number(s): 75.60.Jk, 75.30.Gw, 75.70.Ak

I. INTRODUCTION

Magnetic anisotropy is one of the most important properties of metallic and semiconducting thin-film magnets and has attracted much attention in recent years.[1,2] In magnetic films of cubic systems an in-plane fourfold magnetic anisotropy is expected due to the cubic lattice symmetry but often an additional uniaxial magnetic anisotropy (UMA) is observed to be superimposed on top of the fourfold anisotropy.[3,4] The extra UMA has been attributed to different origins, including a self-shadowing effect occurring during oblique deposition,[5–7] the bonding between film and substrate,[8,9] and the Néel surface effect on a stepped substrate.[10,11] Moreover, ion sputtering has been demonstrated as a reliable tool to control the orientation and strength of UMA by modulating the surface morphology.[12,13]

Prior to the application of thin films for magnetic data storage and spintronic devices, the magnetization-reversal mechanisms and their dependence on the anisotropy symmetry need to be known and controlled in detail. The magnetization-reversal process for combined cubic and uniaxial anisotropies is sensitive to the specific anisotropy geometry and strength.[14,15] Depending on the field orientation, hysteresis curves with one and two steps are observed in various films and explained in terms of nucleation and propagation of 90° and 180° domain walls (DWs).[16,17] Additional information about the relevant reversal mechanisms has been obtained from microscopic imaging of the domain configuration.[15,18] A phenomenological model based on minimizing the magnetic energies has been introduced with DW nucleation energies $\epsilon_{90°}$ for 90° DWs and $\epsilon_{180°}$ for 180° DWs, respectively, in order to account for the observed switching fields.[17] A special magnetic switching process involving three steps can be observed when the additional UMA along the cubic easy axis exceeds the DW nucleation energy $\epsilon_{90°}$.[19,20] Until now, such a switching has been assumed to be mediated by two 90° DW nucleations at the first and the third step and one 180° DW nucleation occurring in between.

Previous work on Fe/MgO(001) films grown at normal incidence revealed a weak UMA along the Fe⟨010⟩ directions.[21] Recently, we successfully relied on ion sputtering to manipulate the strength of the in-plane UMA along the Fe⟨110⟩ directions in Fe/MgO(001).[22] Park *et al.*[23] found that a pronounced UMA can be induced in Fe/MgO(001) by relying on oblique-incidence molecular-beam epitaxy (MBE) growth. Up to now, all of the measured hysteresis loops in Fe/MgO(001) only revealed one or two steps.

Here, we report on a detailed study of the magnetization reversal in Fe/MgO(001) films, where the strength and orientation of UMA are altered either by ion sputtering or by oblique-incidence MBE growth. For the latter MBE growth we now also observe three-step hysteresis loops. A mechanism is introduced with two successive DW nucleations to explain the 180° magnetic switching process that occurs for one-step and three-step loops in Fe/MgO(001) films.

II. EXPERIMENT

Three Fe/MgO(001) films were grown in an ultrahigh vacuum (UHV) MBE system with base pressure below 3×10^{-10} mbar. The substrates were first annealed at 700 °C during one hour and held at 150 °C during deposition. Fe films were deposited using an electron-beam gun at a rate of 0.1 Å/s. The Fe films grow according to the well-known Fe(001)[110]‖MgO(001)[100] epitaxial relation with a possible tetragonal distortion resulting from a relatively small lattice mismatch.[24,25] For sample A the incident Fe beam was at an angle of 49° with respect to the surface normal and with azimuthal angle along Fe[010]. During deposition of sample B at normal incidence, the substrate was rotated around the surface normal. The nominal thickness of samples A and B was 15 nm, as monitored by a calibrated quartz-crystal oscillator. The growth geometry for sample C was the same as for sample B but the nominal thickness was 100 nm. Subsequently, sample C was annealed in UHV at 700 °C during one hour and then sputtered with 2 keV Ar^+ ions at an incidence angle of 60° with respect to the surface normal and with azimuth fixed in between Fe[100] and Fe[$1\bar{1}0$]. During sputtering the ion current toward the sample was kept at 4 μA, which corresponds to an ion flux of

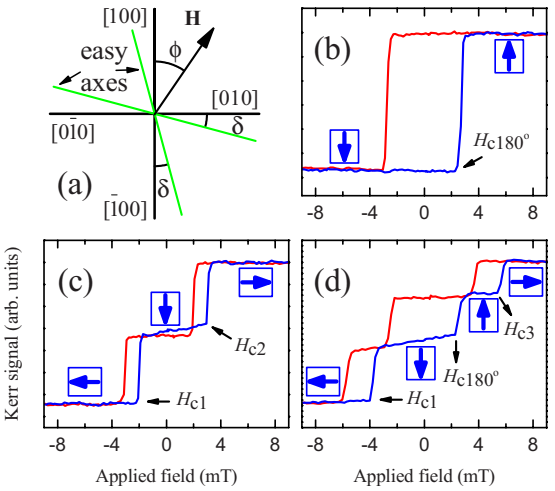

FIG. 1. (Color online) (a) Definition of the angles that are used to describe a film with in-plane cubic anisotropy and an additional UMA. Typical longitudinal MOKE loops for sample A with (b) one step at $\phi=8°$, (c) two steps at $\phi=88°$, and (d) three steps at $\phi=68°$. The blue/dark gray (red/medium gray) curves are for applied fields varying from negative (positive) to positive (negative) saturation. The arrows enclosed by a square represent the orientation of the Fe spins.

2.5×10^{13} ions/cm^2/s. After sputtering for 250 min, the film thickness was reduced to 15 nm, as verified by *ex situ* x-ray reflectometry. Before removing the samples from the vacuum chamber, they were capped with a 4-nm-thick protective Au layer. The magnetic properties of the three samples were measured by the magneto-optical Kerr effect (MOKE). Both longitudinal and transverse loops were obtained for different field orientation ϕ as defined in Fig. 1(a), where the field angle is varied in steps of 5°.

III. EXPERIMENTAL RESULTS AND DISCUSSION

In general, the in-plane UMA, which is superimposed on the cubic anisotropy K_1 of Fe, can be separated into two components: K_{u1} along [010] and K_{u2} along [110].[26] If $K_{u1}\ll K_1$ and $K_{u2}<K_1$, the component K_{u2} rotates the position of the overall easy axes backward with respect to the uniaxial hard axis over an angle δ that is approximately given by $\delta=\frac{1}{2}\sin^{-1}(K_{u2}/K_1)$,[15] as illustrated in Fig. 1(a). As demonstrated below, the orientation and strength of the additional UMA for our Fe/MgO(001) films are strongly affected by the different growth geometries and postgrowth treatments. Consequently, magnetic switching, which is sensitive to the magnetic anisotropy geometry, is quite different for the three investigated samples.

For sample A our experimental results reveal that the oblique deposition results in a considerable UMA along [010]. Three-step loops as well as one-step and two-step loops are observed at different ϕ, as illustrated in Figs. 1(b)–1(d). The evolution of the Fe spin orientation can be easily obtained from the transverse MOKE loop (not shown) and corresponds to the arrows that are enclosed in a square in Figs. 1(b)–1(d). The switching events, which occur for increasing field and $0°<\phi<90°$, are $[\bar{1}00]\rightarrow[100]$ for the one-step loops, $[0\bar{1}0]\rightarrow[\bar{1}00]\rightarrow[010]$ for the two-step loops, and $[0\bar{1}0]\rightarrow[\bar{1}00]\rightarrow[100]\rightarrow[010]$ for the three-step loops.[20] The magnetization switches by 180° for the one-step loops and for the second step of the three-step loops, and by 90° for the other steps.

Up to now, 90° as well as 180° DW nucleations have been invoked to interpret the 90° and 180° magnetic transitions, respectively.[17,20] The coercivity related to the DW nucleation energy can be derived from the energy gain between the local minima at the initial and final easy axes involved in the transition.[17] The theoretical switching fields are obtained as $H_{c1}=(\epsilon_{90°}-K_{u1})/[M(\sin\phi-\cos\phi)]$ for the magnetic switching process $[0\bar{1}0]\rightarrow[\bar{1}00]$, $H_{c2}=(\epsilon_{90°}+K_{u1})/[M(\sin\phi+\cos\phi)]$ for $[\bar{1}00]\rightarrow[010]$, $H_{c3}=(\epsilon_{90°}+K_{u1})/[M(\sin\phi-\cos\phi)]$ for $[100]\rightarrow[010]$, $H_{c4}=(\epsilon_{90°}-K_{u1})/[M(\cos\phi-\sin\phi)]$ for $[010]\rightarrow[100]$, and $H_c=\epsilon_{180°}/[|2M(\cos\phi)|]$ for $[\bar{1}00]\rightarrow[100]$, where M is the magnetization.

For sample A the ϕ dependence of the experimentally observed switching fields can be nicely fitted using the theoretical switching fields, as illustrated in Fig. 2(a), provided we assume the observed switching fields correspond to the theoretically predicted switching fields H_{c1}, H_{c2}, and H_{c3}, as indicated in Figs. 1(c) and 1(d). It is important to note that in Fig. 2 the experimental switching fields corresponding to H_{c2} for the two-step loops are represented by circles. On the other hand, the experimentally observed 180° magnetic transitions, which we surprisingly can fit as well using the theoretical expression for H_{c2}, are represented by diamonds. The fitting in Fig. 2(a) results in the parameters $K_{u1}/M=2.70\pm0.02$ mT and $\epsilon_{90°}/M=0.61\pm0.02$ mT, where $K_{u1}>\epsilon_{90°}$ is the necessary condition for the occurrence of three-step loops.[20]

Following Refs. 17 and 20 we also try to describe the experimental switching field $H_{c180°}$ [diamonds in Fig. 2(a)], which corresponds to a 180° magnetic transition, in terms of 180° DW nucleation. Using the corresponding theoretical switching field H_c, we obtain the very poor fit represented by the green (light gray) curve in the two insets of Fig. 2(a). At $\phi=0°$ (one-step loops), H_c reaches a minimum while $H_{c180°}$ reveals a peak. For $45°<\phi<77°$ and for $103°<\phi<135°$, where the three-step loops occur (see below), both H_c and $H_{c180°}$ increase toward 90° but H_c has a slope that strongly exceeds the experimental slope. 180° DW nucleation clearly fails to describe the observed angular dependence of $H_{c180°}$.

As indicated above, we surprisingly find that the theoretical expression for H_{c2}, which corresponds to a 90° DW nucleation, allows us to nicely fit the $H_{c180°}$ data. As described in more detail below, this can be understood by the fact that the 180° magnetic transitions in our sample A in fact consist of a 90° magnetic transition at H_{c2}, which is immediately followed by another 90° magnetic transition at the same field H_{c2}.

In order to confirm that this phenomenon is independent of the anisotropy geometry of the Fe/MgO(001) films, we now turn to the ϕ dependence of the switching fields for samples B and C. The results are presented in Figs. 2(b) and

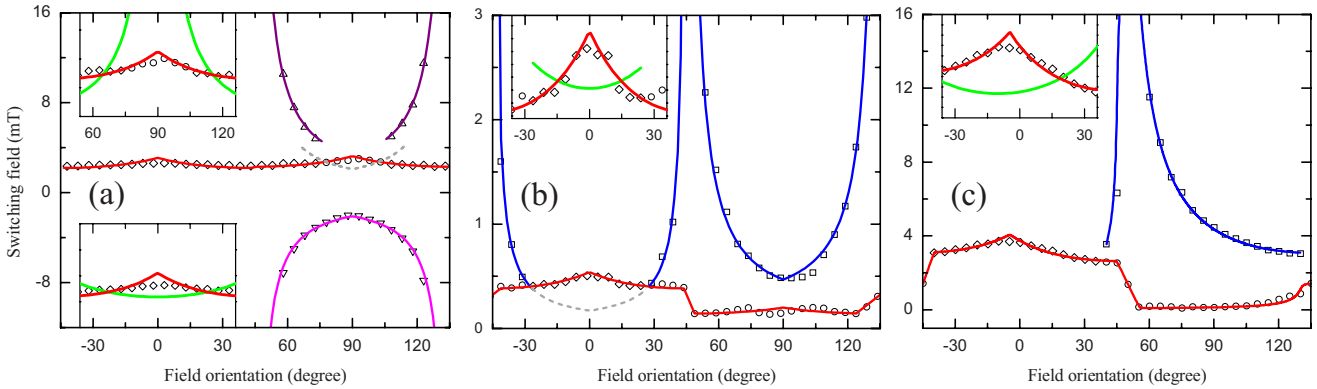

FIG. 2. (Color online) The experimentally observed switching fields H_{c1} (inverted triangles), H_{c2} (dots), H_{c3} (triangles), H_{c4} (squares), and $H_{c180°}$ (diamonds) as a function of the field orientation ϕ, and the corresponding theoretical curves for H_{c1} (magenta), H_{c2} (red), H_{c3} (purple), H_{c4} (blue), and the "virtual" H_{c4} (dashed gray) for (a) sample A, (b) sample B, and (c) sample C. In the insets we present a more detailed view of the fit of the measured $H_{c180°}$, which is observed for the one-step loops and for the second step of the three-step loops by the theoretical expressions for H_{c2} (red/medium gray) and H_c (green/light gray).

2(c). Only one-step and two-step loops are observed. As discussed in our recent publication,[22] the switching route for the two-step loops appearing in samples B and C is $180°-\delta \rightarrow 90°+\delta \rightarrow -\delta$ for $-\delta < \phi < 45°$, which is different from the path for sample A. When $\delta=0$, i.e., $K_{u2}=0$, the experimental switching fields for this type of two-step loop should correspond to the above derived expressions for H_{c2} and H_{c4}. In case $\delta \neq 0$, i.e., $K_{u2} \neq 0$, the theoretical expressions need to be extended. In this more universal case the total energy E for an arbitrary single domain spin orientation can then be written as $E=(K_1/4)\sin^2 2\theta + K_{u1}\sin^2\theta + K_{u2}\sin^2(\theta+\pi/4) - MH\cos(\phi-\theta)$. Consequently, the energies of the single domain states at the local minima are $E_{-\delta}=K_{u1}\sin^2\delta - MH\cos(\phi+\delta)$, $E_{90°+\delta}=K_{u1}\cos^2\delta - MH\sin(\phi-\delta)$, $E_{180°-\delta}=K_{u1}\sin^2\delta + MH\cos(\phi+\delta)$, and $E_{270°+\delta}=K_{u1}\cos^2\delta + MH\sin(\phi-\delta)$. Therefore, for the magnetic switching processes $180°-\delta \rightarrow 90°+\delta$ and $90°+\delta \rightarrow -\delta$ the domain-wall nucleation energies are $\epsilon_{90°-2\delta}=E_{180°-\delta}-E_{90°+\delta}$ for $H=H_{c2}$ and $\epsilon_{90°+2\delta}=E_{90°+\delta}-E_{-\delta}$ for $H=H_{c4}$, respectively. We then obtain the following expressions for the switching fields:

$$H_{c2}=\frac{\epsilon_{90°-2\delta}+K_{u1}(\cos^2\delta-\sin^2\delta)}{M[\cos(\phi+\delta)+\sin(\phi-\delta)]},$$

$$H_{c4}=\frac{\epsilon_{90°+2\delta}-K_{u1}(\cos^2\delta-\sin^2\delta)}{M[\cos(\phi+\delta)-\sin(\phi-\delta)]}.$$

For sample B the two switching fields (H_{c2}, H_{c4}) have a dependence on ϕ that is symmetric about $\langle 100\rangle$. Moreover, the angular dependence of H_{c2} reveals a clear and abrupt step when crossing $\langle 110\rangle$, as illustrated in Fig. 2(b). We conclude that sample B has a small in-plane UMA along [010].[17] The fitting parameters are $K_{u1}/M=0.19\pm0.01$ mT and $\epsilon_{90°}/M=0.36\pm0.01$ mT. Because $K_{u1}<\epsilon_{90°}$, three-step loops cannot be observed.

For sample C we find that after Ar^+ ion sputtering the UMA has components along [010] as well as along [110]. The overall easy axes are observed to deviate from $\langle 100\rangle$ by an angle $\delta=3°$, i.e., $K_{u2}/K_1 \approx 0.1$. From the comparison between theory and experiment in Fig. 2(c) we find that the UMA component along [010] and the DW nucleation energies are $K_{u1}/M=1.69\pm0.02$ mT, $\epsilon_{90°-2\delta}/M=1.83\pm0.02$ mT, and $\epsilon_{90°+2\delta}/M=2.29\pm0.02$ mT, respectively. Because K_{u1} is comparable to $\epsilon_{90°-2\delta}$, the path $270°+\delta \rightarrow -\delta \rightarrow 90°+\delta$ is energetically more favorable when compared to the counterclockwise path via $180°-\delta$ for the whole range of angles $45° < \phi < 135°$. Consequently, both H_{c2} and H_{c4} change monotonously within this range.

We again try to describe $H_{c180°}$ for the one-step loops of samples B and C in terms of 180° DW nucleation, as illustrated in the insets of Figs. 2(b) and 2(c), respectively. The theoretical curves clearly disagree with our experimental observations. From the fitting results for the three samples with different anisotropy geometry and strength we conclude that $90°\pm2\delta$ magnetic transitions in Fe/MgO(001) films are mediated by $90°\pm2\delta$ DW nucleation but 180° magnetization reorientations are not mediated by 180° DW nucleation.

IV. MAGNETIZATION-REVERSAL MECHANISM

What is the physical mechanism that dominates the 180° magnetic reversal in our experiments? Based on the obtained values for the fitting parameters K_{u1} and $\epsilon_{90°}$, we plot the

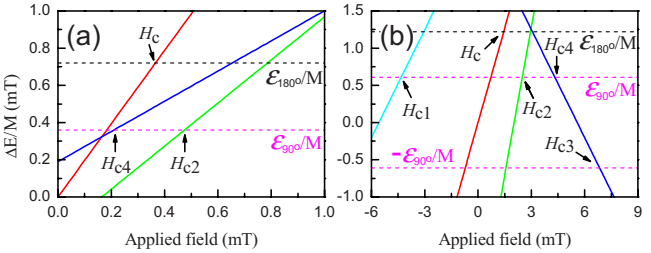

FIG. 3. (Color online) Energy differences $\Delta E_{180°\rightarrow0°}$ (red), $\Delta E_{270°\rightarrow180°}$ (cyan), $\Delta E_{180°\rightarrow90°}$ (green), and $\Delta E_{90°\rightarrow0°}$ (blue) as a function of the applied field for (a) sample B at $\phi=10°$ and (b) sample A at $\phi=65°$, respectively.

energy difference between the relevant easy axes as a function of the applied field in Fig. 3(a) for sample B at $\phi=10°$ and in Fig. 3(b) for sample A at $\phi=65°$, respectively. In the previously adopted model the energy difference between 180° and 0° is treated in terms of *one single barrier* and 180° DW nucleation occurs at H_c when $\Delta E_{180°\to 0°}=\epsilon_{180°}$, where $\epsilon_{180°}$ is assumed to correspond to $2\epsilon_{90°}$.[20] According to our analysis the switching between $[\bar{1}00]$ and [100] is governed by *two separate energy barriers* that need to be overcome between $[\bar{1}00]$ and [010] and between [010] and [100], respectively. The switching then corresponds to two 90° DW nucleation processes. The energy barrier for the transition from $[\bar{1}00]$ and [010] becomes $\Delta E_{180°\to 90°}=\epsilon_{90°}$ at H_{c2}. However, since $\Delta E_{90°\to 0°}$ already exceeds $\epsilon_{90°}$ at H_{c2}, the domains along [010] are unstable and cannot grow. Therefore, a second nucleation of domains along the final [100] remanent direction occurs at H_{c2} and the two successive 90° DW nucleations appear as one single step in the MOKE loops. In case $\delta\neq 0$, this process consists of a $90°-2\delta$ DW nucleation and a subsequent $90°+2\delta$ DW nucleation or vice versa. Based on our model, the experimental switching fields $H_{c180°}$ for all three samples are fitted by the expressions for H_{c2} in Figs. 2(a)–2(c) and the insets. This way, all switching fields for the three types of loops can be nicely fitted by consistently using for a given sample the same $\epsilon_{90°\pm 2\delta}$ and K_{u1} values for the complete range of angles.

In case of two successive DW nucleations, H_{c4} is not an experimental observable switching field. H_{c4} only indicates $\Delta E_{90°+\delta\to -\delta}=\epsilon_{90°+2\delta}$. We have plotted in Figs. 2(a) and 2(b) the "virtual" H_{c4} values for samples A and B. When $0°<\phi<45°$, the two successive DW nucleations appear as one-step loops for $H_{c2}>H_{c4}$ [also see Fig. 3(a)]. For $H_{c2}<H_{c4}$ the magnetization loops reveal a two-step behavior with two separate 90° DW nucleations occurring at H_{c2} and H_{c4}, respectively. When $45°<\phi<90°$ and $K_{u1}>\epsilon_{90°}$, the magnetization switches from $[0\bar{1}0]$ to $[\bar{1}00]$ at H_{c1}, where $\Delta E_{270°\to 180°}=\epsilon_{90°}$. Because $\Delta E_{90°\to 0°}$ decreases with increasing applied field and becomes $\epsilon_{90°}$ at H_{c4} [see Fig. 3(b)], two successive DW nucleations appear for $H_{c2}<H_{c4}$. Upon further increasing the field, $\Delta E_{90°\to 0°}$ becomes negative and finally reaches $-\epsilon_{90°}$ at a coercive field H_{c3}, where the magnetization switches backward from [100] to [010]. As a result, the magnetization loops contain three steps. For $H_{c2}>H_{c4}$ the domains aligned along 90° are energetically stable when the applied field exceeds H_{c2}, resulting in two-step loops.

By comparing the expressions for H_{c2} and H_{c4} the field orientation for the occurrence of one-step or three-step loops can be obtained. For the simple case $\delta=0$, the condition $\tan\phi<K_{u1}/\epsilon_{90°}$ needs to be satisfied, where $0<\phi<45°$ for the one-step loops and $45°<\phi<90°$ for the three-step loops, respectively. Our model predicts that the ranges of angles for which a one-step loop should be observed are $-45°<\phi<45°$, $-28°<\phi<28°$, and $-43°<\phi<36°$ for samples A, B, and C, respectively. The critical angles separating the occurrence of two-step and three-step loops are $\phi=90°\pm 13°$ for sample A. Our model calculations are obviously in excellent agreement with the experimental observations. Here, we also want to point out that the phase diagram presented in Fig. 2 in Ref. 20 remains valid for both

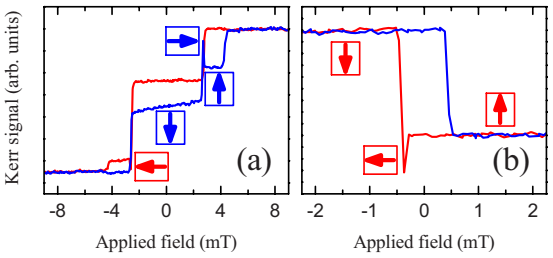

FIG. 4. (Color online) (a) The longitudinal magnetization loop of sample A at $\phi=76°$ and (b) the transverse magnetization loop of sample B at $\phi=29°$ reveal overshoots near the critical angles for the field orientation.

$K_{u1}<\epsilon_{90°}$ and $K_{u1}>\epsilon_{90°}$. This can be linked to the fact that our magnetization reversal consisting of two successive 90° transitions is to a certain extent similar to the assumption that "a 180° DW is equivalent to two 90° DWs very weakly coupled together" in Ref. 20. Both the model introduced in Ref. 20 and our adapted version of the model reveal that the coercivity depends on the DW nucleation energies as well as on the strength of the anisotropy. The DW nucleation energy mainly results from the DW pinning by defects in the film and by interfacial roughness.

Introducing two successive DW nucleations allows us to consistently interpret the 180° magnetization reorientation in our samples. Since the DWs induced during the first nucleation are energetically unstable, it should be very hard to experimentally observe these intermediate domains. In real films, however, the DW nucleation energy needs to be described in terms of a (narrow) distribution of energies and the DW propagation velocity is finite,[27,28] implying magnetic switching is not as sharp as predicted by theory. As illustrated by the longitudinal MOKE loop in Fig. 4(a), our experimental observations are consistent with the existence of intermediate states in the three-step loops of sample A close to the critical angles separating the occurrence of two-step and three-step loops. The blue curve (increasing field) reveals an overshoot for the magnetic switching from $[\bar{1}00]$ to [100], which indicates that the Fe spins align along [010] before jumping to [100]. The red curve (decreasing field) reveals a similar feature. We also note that the second intermediate state in the blue curve in Fig. 4(a) is not collinear with the first intermediate state in the red curve and vice versa, which is different from the loop shown in Fig. 1(d). The noncollinearity in the loop implies that not all spins switch from $[\bar{1}00]$ to [010] and then to [100] but some of the spins remain aligned along [010]. This points to the coexistence of magnetic switching processes with both two-step and three-step loops. The overshoot gradually becomes less pronounced when moving a few degrees away from the critical angles. In sample B we observe a mixture of one-step and two-step loops, as illustrated by the transverse MOKE loop in Fig. 4(b). The red curve of the transverse MOKE loop indicates the presence of two separate 90° DW nucleations while the blue curve corresponds according to our model to two successive and indistinguishable DW nucleations. Experimentally, the transition between two reversal mechanisms does not take place at one single critical point as pre-

dicted by theory but extends over a small finite range of angles. This obviously deserves further experimental and theoretical study. Time-resolved MOKE may be an appropriate tool to detect the ultrafast magnetization dynamics and enable to reveal more details about the intermediate domain formation in the process of two successive DW nucleations.

V. CONCLUSIONS

We have introduced a magnetic-reversal mechanism with two successive domain-wall nucleations in order to explain the 180° magnetization reversal in Fe/MgO(001) films with fourfold in-plane magnetic anisotropy and an additional uniaxial anisotropy. The orientation and the strength of the extra uniaxial anisotropy for Fe/MgO(001) films can be experimentally altered using different growth conditions and postgrowth treatments. Our model consistently accounts quantitatively for the observed switching fields for all field orientations and correctly predicts the critical angles of the field orientation that separate the occurrence of magnetization loop with different shapes. Predictions based on 180° domain-wall nucleation clearly fail to provide a correct description of the experimental observations.

ACKNOWLEDGMENTS

Financial support was provided by the Fund for Scientific Research-Flanders (FWO) as well as by the Flemish Concerted Action (GOA) and the Belgian Interuniversity Attraction Poles (IAP) research programs.

[1] M. T. Johnson, P. J. H. Bloemen, F. J. A. den Broeder, and J. J. de Vries, Rep. Prog. Phys. **59**, 1409 (1996).
[2] C. Gould, K. Pappert, G. Schmidt, and L. W. Molenkamp, Adv. Mater. (Weinheim, Ger.) **19**, 323 (2007).
[3] C. Gould, C. Rüster, T. Jungwirth, E. Girgis, G. M. Schott, R. Giraud, K. Brunner, G. Schmidt, and L. W. Molenkamp, Phys. Rev. Lett. **93**, 117203 (2004).
[4] C. S. Tian, D. Qian, D. Wu, R. H. He, Y. Z. Wu, W. X. Tang, L. F. Yin, Y. S. Shi, G. S. Dong, X. F. Jin, X. M. Jiang, F. Q. Liu, H. J. Qian, K. Sun, L. M. Wang, G. Rossi, Z. Q. Qiu, and J. Shi, Phys. Rev. Lett. **94**, 137210 (2005).
[5] S. Cherifi, R. Hertel, A. Locatelli, Y. Watanabe, G. Potdevin, A. Ballestrazzi, M. Balboni, and S. Heun, Appl. Phys. Lett. **91**, 092502 (2007).
[6] J. L. Bubendorff, S. Zabrocki, G. Garreau, S. Hajjar, R. Jaafar, D. Berling, A. Mehdaoui, C. Pirri, and G. Gewinner, Europhys. Lett. **75**, 119 (2006).
[7] Y. Shim and J. G. Amar, Phys. Rev. Lett. **98**, 046103 (2007).
[8] J. W. Freeland, I. Coulthard, W. J. Antel, and A. P. J. Stampfl, Phys. Rev. B **63**, 193301 (2001).
[9] H. B. Zhao, D. Talbayev, G. Lüpke, A. T. Hanbicki, C. H. Li, M. J. van't Erve, G. Kioseoglou, and B. T. Jonker, Phys. Rev. Lett. **95**, 137202 (2005).
[10] J. Chen and J. L. Erskine, Phys. Rev. Lett. **68**, 1212 (1992).
[11] Y. Z. Wu, C. Won, and Z. Q. Qiu, Phys. Rev. B **65**, 184419 (2002).
[12] R. Moroni, D. Sekiba, F. Buatier de Mongeot, G. Gonella, C. Boragno, L. Mattera, and U. Valbusa, Phys. Rev. Lett. **91**, 167207 (2003).
[13] F. Bisio, R. Moroni, F. Buatier de Mongeot, M. Canepa, and L. Mattera, Phys. Rev. Lett. **96**, 057204 (2006).
[14] K. Pappert, S. Hümpfner, J. Wenisch, K. Brunner, C. Gould, G. Schmidt, and L. W. Molenkamp, Appl. Phys. Lett. **90**, 062109 (2007).
[15] C. Daboo, R. J. Hicken, E. Gu, M. Gester, S. J. Gray, D. E. P. Eley, E. Ahmad, J. A. C. Bland, R. Ploessl, and J. N. Chapman, Phys. Rev. B **51**, 15964 (1995).
[16] Z. H. Wang, G. Cristiani, H. U. Habermeier, and J. A. C. Bland, Phys. Rev. B **72**, 054407 (2005).
[17] R. P. Cowburn, S. J. Gray, J. Ferré, J. A. C. Bland, and J. Miltat, J. Appl. Phys. **78**, 7210 (1995).
[18] F. Y. Yang, C. H. Shang, C. L. Chien, T. Ambrose, J. J. Krebs, G. A. Prinz, V. I. Nikitenko, V. S. Gornakov, A. J. Shapiro, and R. D. Shull, Phys. Rev. B **65**, 174410 (2002).
[19] S. van Dijken, G. Di Santo, and B. Poelsema, Phys. Rev. B **63**, 104431 (2001).
[20] R. P. Cowburn, S. J. Gray, and J. A. C. Bland, Phys. Rev. Lett. **79**, 4018 (1997).
[21] J. L. Costa-Krämer, J. L. Menéndez, A. Cebollada, F. Briones, D. García, and A. Hernando, J. Magn. Magn. Mater. **210**, 341 (2000).
[22] Q. F. Zhan, S. Vandezande, C. Van Haesendonck, and K. Temst, Appl. Phys. Lett. **91**, 122510 (2007).
[23] Y. Park, E. E. Fullerton, and S. D. Bader, Appl. Phys. Lett. **66**, 2140 (1995).
[24] T. Urano and T. Kanaji, J. Phys. Soc. Jpn. **57**, 3403 (1988).
[25] H. Fuke, A. Sawabe, and T. Mizoguchi, Jpn. J. Appl. Phys. **32**, L1137 (1993).
[26] K. Pappert, C. Gould, M. Sawicki, J. Wenisch, K. Brunner, G. Schmidt, and L. W. Molenkamp, New J. Phys. **9**, 354 (2007).
[27] E. Arenholz and K. Liu, Appl. Phys. Lett. **87**, 132501 (2005).
[28] Y. Nakatani, A. Thiaville, and J. Miltat, Nature Mater. **2**, 521 (2003).